Journal of ELECTRONIC MATERIALS
DOI: 10.1007/s11664-012-1917-9

Seebeck Enhancement Through Miniband Conduction in III–V Semiconductor Superlattices at Low Temperatures

JE-HYEONG BAHK,[1,2] RAMIN BANAN SADEGHIAN,[1] ZHIXI BIAN,[1] and ALI SHAKOURI[1]

1.—Department of Electrical Engineering, University of California, Santa Cruz, CA 95064, USA.
2.—e-mail: jhbahk@soe.ucsc.edu

We present theoretically that the cross-plane Seebeck coefficient of InGaAs/InGaAlAs III–V semiconductor superlattices can be significantly enhanced through miniband transport at low temperatures. The miniband dispersion curves are calculated by self-consistently solving the Schrödinger equation with the periodic potential, and the Poisson equation taking into account the charge transfer between the two layers. Boltzmann transport in the relaxation-time approximation is used to calculate the thermoelectric transport properties in the cross-plane direction based on the modified density of states and group velocity. It is found that the cross-plane Seebeck coefficient can be enhanced more than 60% over the bulk values at an equivalent doping level at 80 K when the Fermi level is aligned at an edge of the minibands. Other thermoelectric transport properties are also calculated and discussed to further enhance the thermoelectric power factor.

Key words: Thermoelectric, superlattice, miniband transport, III–V semiconductors

INTRODUCTION

The efficiency of thermoelectric energy conversion is directly related to the dimensionless thermoelectric figure of merit, $ZT = S^2\sigma T/(\kappa_e + \kappa_l)$, of the materials used, where S is the Seebeck coefficient, σ is the electrical conductivity, T is the absolute temperature, and κ_e and κ_l are the electronic and lattice thermal conductivities, respectively. In recent years, significant enhancements in ZT have been achieved particularly by reducing the lattice thermal conductivity with added interfaces via superlattice structures[1,2] and nanocomposites.[3–5] However, the numerator in ZT, $S^2\sigma$, the so-called thermoelectric power factor, has not been reported to be noticeably enhanced by superlattices.

Hicks and Dresselhaus predicted theoretically improved thermoelectric power factors in low-dimensional materials such as quantum wells in 1993.[6] This improvement is mainly due to the quantized states in the directions perpendicular to the potential barrier, which create sharp features in the electronic density of states (DOS). Sharp features in the DOS increase the asymmetry between hot and cold electron transport, in favor of hot electrons, increasing the average amount of energy and heat carried by electrons and thus enhancing the Seebeck coefficient over those of the bulk material. The transport in their work is in the in-plane direction of the quantum wells that are perfectly confined by ideal barriers.

In the cross-plane direction of superlattices, Shakouri et al. suggested that tall-barrier, highly degenerate superlattice heterostructures could achieve thermoelectric power factors an order of magnitude higher than bulk values.[7] This improvement is due to the filtering of hot electrons with energy above the barrier height in the course of thermionic emission. The barrier is assumed to be sufficiently thick, and the superlattice period is much larger than the mean free path of carriers so that miniband transport does not occur in their work.

When the superlattice period is much smaller than the mean free path of charge carriers, minibands are formed by coherent multiple interferences by the

(Received July 17, 2011; accepted January 5, 2012)

Published online: 08 February 2012

periodic superlattice potential. Friedman used a simple sinusoidal model of minibands to show that the Seebeck coefficient is significantly increased at the miniband extrema.[8] Vashaee et al. suggested that the thermoelectric power factor can be significantly enhanced through the transport in multiple minibands in particular when the lateral momentum is not conserved.[9] However, the variation of group velocity by the miniband transport was ignored in the work, and thus the power factor enhancement was overestimated. Recently, Bian et al. accurately calculated the variation of group velocity and the Lorenz number in miniband transport to estimate the thermoelectric figure of merit of III–V semiconductor superlattices at high temperatures above room temperatures.[10] A self-consistent method to incorporate the potential bending due to charge transfer between the barrier and well layers in the miniband calculations was also proposed in the paper.

InGaAs/InGaAlAs superlattices have been extensively studied due to their usefulness in various applications such as thermoelectric energy conversion,[11,12] and infrared detection,[13] so that their material properties such as band offsets are well known.[14] Since recent advances in material growth techniques such as molecular beam epitaxy enable growth of high-quality multiple quantum wells and superlattices of III–V semiconductors,[15] these superlattices are well suited to study of miniband transport and applications. The performance of the III–V superlattices has been successfully explained by miniband transport calculations previously.[9]

In this work, we extend the method proposed in Ref. 9 to theoretically investigate the thermoelectric transport via minibands in InGaAlAs/InGaAs III–V semiconductor superlattices at low temperatures. We calculate the thermoelectric power factors in various conditions of the III–V superlattices, and show that the Seebeck coefficient can be significantly enhanced by utilizing the sharp features in the DOS in the miniband transport in particular at low temperatures when the electron distribution that contributes to conduction is sufficiently narrow. The electrical conductivity reduction due to the suppressed group velocity in the miniband transport is also discussed.

THEORY

The miniband structure of superlattices is calculated based on the Kronig–Penney model in the one-dimensional cross-plane direction. A period of the superlattice, d, is divided into small-size elements in the cross-plane direction, i.e., z-direction. In each element, the potential $V(z)$ is assumed to be constant, and the wave function solution of the Schrödinger equation can be written as

$$\psi_i(z) = A_i \exp(ik_i z) + B_i \exp(-ik_i z), \tag{1}$$

where A_i and B_i are the coefficients determined by the boundary conditions depicting continuity of the wave and its derivative, and k_i is the wavevector given by

$$k_i^2 = \frac{2m^*}{\hbar^2}(E_i - V(z)), \tag{2}$$

where m^* is the effective mass, and E_i is the electron eigenenergy. Note that the wave function is a sinusoidal function where E_i is larger than the potential $V(z)$, and is an exponentially decaying function where E_i is smaller than the potential $V(z)$, i.e., inside the barrier.

According to Bloch's theorem, the wave functions can differ by a certain phase after each period step when there are multiple periods[16]

$$\psi_i(z+d) = \psi_i(z)\exp(iq_n d), \tag{3}$$

where q_n is the Bloch wavevector that satisfies the periodic boundary condition for N periods of superlattices given by

$$q_n N d = 2\pi n, \tag{4}$$

where n is any integer between $-N/2$ and $N/2$. For each n and i, a pair of the wave function ψ_{ni} and its corresponding eigenenergy E_{ni} are found to satisfy the Schrödinger equation, and thus E_{ni} is a smoothly changing function of q_n, which forms the ith miniband. There is a forbidden energy gap between each adjacent miniband when confinement is strong.

The DOS of the superlattice is modified in the z-direction due to the miniband formation[9]

$$\rho_{\mathrm{DOS}}(E) = \sum_n \sum_i \frac{m^*}{\pi\hbar^2 d}(1 + 2\alpha(E - E_{ni}))u(E - E_{ni}), \tag{5}$$

where α is the nonparabolicity from the in-plane dispersion relation, and $u(E)$ is the unit step function. The Fermi level E_{F} is then found using Eq. 5 and the Fermi–Dirac distribution function $f_0(E) = 1/(1 + \exp((E - E_{\mathrm{F}})/k_{\mathrm{B}}T))$ from the following equation:

$$N_{\mathrm{d}} = \int \rho_{\mathrm{DOS}}(E) f_0(E)\mathrm{d}E, \tag{6}$$

where N_{d} is the average doping density in the superlattice given by

$$N_{\mathrm{d}} = \frac{N_{\mathrm{d,well}} d_{\mathrm{well}} + N_{\mathrm{d,barrier}} d_{\mathrm{barrier}}}{d_{\mathrm{well}} + d_{\mathrm{barrier}}}, \tag{7}$$

where $N_{\mathrm{d,well}}$ and $N_{\mathrm{d,barrier}}$ are the doping densities in the well and barrier layers, and d_{well} and d_{barrier} are the thicknesses of the well and barrier layers, respectively.

The local carrier density $n_e(z)$ at a position z is determined by the local DOS given by

$$\rho^*_{\mathrm{DOS}}(E,z) = \sum_n \sum_i |\psi_{ni}(z)|^2 \frac{m^*}{\pi\hbar^2 d} (1 + 2\alpha(E - E_{ni}))u(E - E_{ni}), \tag{8}$$

where the spatial distribution of the normalized wave functions is included in the DOS. Hence,

$$n_e(z) = \int \rho^*_{\mathrm{DOS}}(E,z) f_0(E)\mathrm{d}E. \tag{9}$$

Subsequently, the potential bending due to the charge redistribution can be calculated from the Poisson equation[16]

$$\frac{\mathrm{d}}{\mathrm{d}z}\left(\varepsilon(z)\frac{\mathrm{d}}{\mathrm{d}z}\right)\phi(z) = -e\left[n_e(z) - N_{\mathrm{d}}^+(z)\right], \tag{10}$$

where e is electron charge, $\varepsilon(z)$ is the electron permittivity, and $N_{\mathrm{d}}^+(z)$ is the concentration of ionized dopants as a function of position. The potential bending is then used to update the potential profile

$$V(z) = e\phi(z) + \Delta E_{\mathrm{C}}(z), \tag{11}$$

where $\Delta E_{\mathrm{C}}(z)$ is the conduction-band offset, the original potential profile before the charge transfer. Since the potential profile has been changed, the wave functions and the eigenenergies need to be recalculated using Eqs. 1–3. Thus, iterations are performed until both the potential and the miniband structures converge.

The group velocity of each eigenstate along the cross-plane direction can be calculated from the dispersion curves of the minibands[16]

$$v_{g,ni} = \frac{1}{\hbar}\frac{\partial E_{ni}}{\partial q_n}. \tag{12}$$

Then, the average group velocity in the z-direction at a given energy E can be found using Eq. 12 as

$$v_g^2(E) = \frac{\sum_n \sum_i v_{g,ni}^2 u(E - E_{ni})}{\sum_n \sum_i u(E - E_{ni})}. \tag{13}$$

Finally, the electrical conductivity σ and the Seebeck coefficient S can be calculated from the Boltzmann transport equation with the relaxation-time approximation. They are all integral functions of the differential conductivity that is determined by Eqs. 5, 13, and the electron momentum relaxation time $\tau(E)$[17]

$$\sigma_d(E) = e^2\tau(E)v_g^2(E)\rho_{\mathrm{DOS}}(E)\left(-\frac{\partial f_0(E)}{\partial E}\right), \tag{14}$$

$$\sigma = \int_0^\infty \sigma_d(E)\mathrm{d}E, \tag{15}$$

$$S = \frac{1}{eT}\frac{\int_0^\infty \sigma_d(E)(E - E_{\mathrm{F}})\mathrm{d}E}{\int_0^\infty \sigma_d(E)\mathrm{d}E}. \tag{16}$$

In this work, the bulk electron momentum relaxation time is used for the superlattices, which may place uncertainty in the transport calculations.

RESULTS AND DISCUSSION

In this paper, we choose $(\mathrm{InGaAs})_{0.9}(\mathrm{InAlAs})_{0.1}$ lattice-matched to InP substrate as a barrier material, which has conduction-band offset of 50 meV at 80 K, with InGaAs lattice-matched to InP as a well material. This band offset is still sufficiently large considering the small $k_{\mathrm{B}}T$ at such a low temperature. A low temperature (80 K) is chosen because a large Seebeck enhancement can be obtained when the energy distribution is sufficiently narrow so that most electrons are guaranteed to see the very narrow sharp features in the DOS.

Figure 1 shows the miniband dispersion curves calculated for the InGaAs/InGaAlAs superlattices with varying barrier widths from 20 nm to 5 nm while the well width is fixed to be 20 nm. The mean free path of electrons in the bulk materials (~100 nm at 80 K) is much larger than the periods of the superlattices, which satisfies the requirement to form minibands. As shown in Fig. 1, the width and position of minibands can be tuned by changing the barrier width. The widths of the minibands (along the y-axis) increase, and the position of the minibands is shifted down as the barrier width is decreased because the confinement becomes weaker with a narrower barrier. At very high-energy region, minibands almost disappear, and only zone folding of a bulk-like dispersion curve is observed.

Figure 2 shows the final potential profile after charge transfer in comparison with the initial potential, and the Fermi level across a single period of the superlattice. In Fig. 2, both well and barrier layers were uniformly doped by 5×10^{17} cm^{-3} as an example. Thus, there is charge transfer from the barrier regions to well regions to align the Fermi level the same along the whole period. As a result, the potential in the well region and in its vicinity is bent up symmetrically. The modified potential profile affects the quantized levels and dispersion curves of minibands. Therefore, a self-consistent iterative calculation is necessary to find the final miniband structure and transport properties accurately.

DOS for superlattices with well width of 20 nm and three different barrier widths of 20 nm, 10 nm,

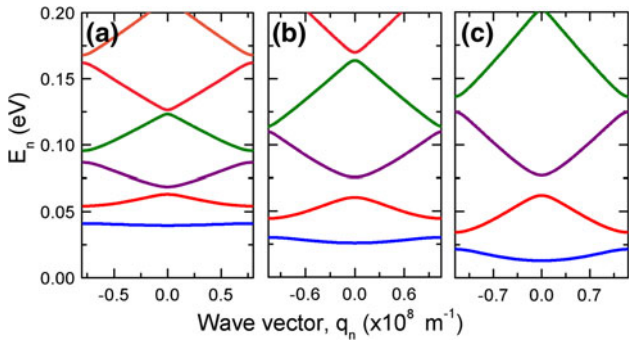

Fig. 1. Dispersion curves of minibands in InGaAs/InGaAlAs (10% Al) superlattices with well/barrier widths of (a) 20 nm/20 nm, (b) 20 nm/10 nm, and (c) 20 nm/5 nm (color figure online).

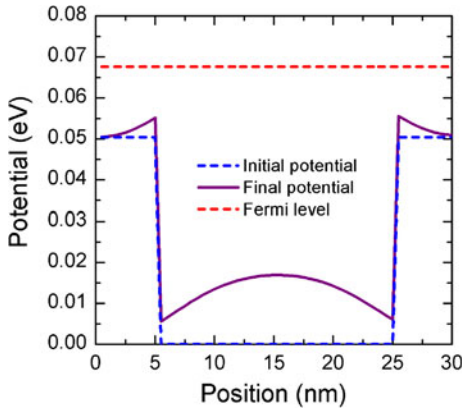

Fig. 2. Potential profile and Fermi level of the 20 nm/10 nm InGaAs/InGaAlAs (10% Al) superlattice uniformly doped by 5×10^{17} cm^{-3}. Both the initial potential and the final potential after band bending due to charge transfer are shown (color figure online).

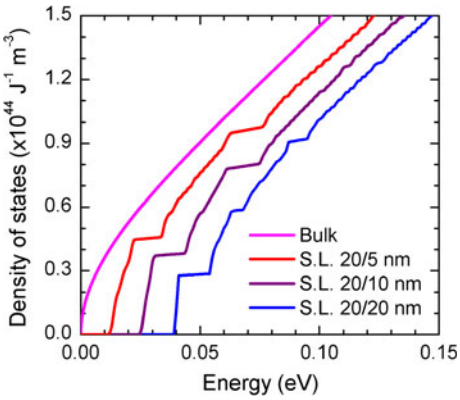

Fig. 3. Density of states of InGaAs/InGaAlAs (10% Al) superlattices with three different barrier widths in comparison with that of bulk InGaAs (color figure online).

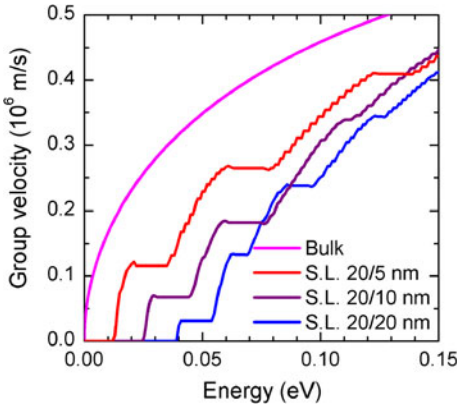

Fig. 4. Electron group velocity in the cross-plane direction of InGaAs/InGaAlAs (10% Al) superlattices with three different barrier widths in comparison with that of bulk InGaAs (color figure online).

and 5 nm were calculated at various doping levels using Eq. 5. Both well and barrier layers are assumed to be doped uniformly with the same doping density. Figure 3 shows the DOS of the superlattices in comparison with that of the well bulk material at the uniform doping density of 7×10^{17} cm^{-3}. Due to the miniband formation, step-like DOS are observed for the superlattices with near-flat DOS in the forbidden gaps between minibands. Slight increase of the DOS in the forbidden gap is due to the nonparabolic band in the in-plane direction. Inside each miniband, the DOS sharply increases with energy, and can be approximated as an inverse cosine function.[8] The DOS increase more rapidly with energy for wider barrier superlattices because minibands are narrower. Bulk has the largest DOS at a given energy, and narrower-barrier superlattices have larger DOS with values closer to the bulk.

Group velocity in the cross-plane direction was calculated using Eq. 13 and is shown in Fig. 4 for the three different barrier widths. Wider barrier reduces group velocity more because the miniband is flatter and narrower. This also means that thicker barriers are harder for electrons to pass through because tunneling becomes less probable. It is noted that the superlattice group velocity is more than an order of magnitude slower than that in bulk near the lowest miniband. This implies that mobility or electrical conductivity can be significantly low at low doping densities where most of the electron transport occurs through the lowest miniband.

Finally, the Seebeck coefficient, electrical conductivity, and power factor were calculated using Eqs. 14–16 from the miniband structures at 80 K, and are shown in Figs. 5, 6, and 7, respectively. Seebeck coefficients were significantly enhanced over the bulk values in the miniband transport, as shown in Fig. 5. More than 60% enhancement in Seebeck is observed at high 10^{16} cm^{-3} and low 10^{17} cm^{-3} doping density for 20 nm/20 nm barrier/well width. Oscillatory behavior of Seebeck coefficient with doping density is also observed because the Fermi level position relative to the miniband extrema changes with doping density. Thicker-barrier superlattice shows larger Seebeck enhancement mainly due to the sharper increase of DOS inside the minibands for thicker barriers.

However, there is a trade-off between the Seebeck coefficient and the electrical conductivity in superlattices as well. As one can see in Fig. 6, electrical conductivity decreases as barrier thickness increases, which is more apparent at low-doping region. More than an order of magnitude conductivity reduction is observed for 20 nm and 10 nm barrier widths at the low-doping region. At high-doping regions where the Fermi level is positioned much higher than the barrier, however, the barrier effect becomes less significant and all the transport properties approach the bulk curves. Due to the suppressed group velocity and electrical conductivity, the power factor cannot be enhanced at low doping levels below a few 10^{17} cm^{-3} even though the Seebeck enhancement is largest at those doping levels. The maximum power factor is found to be

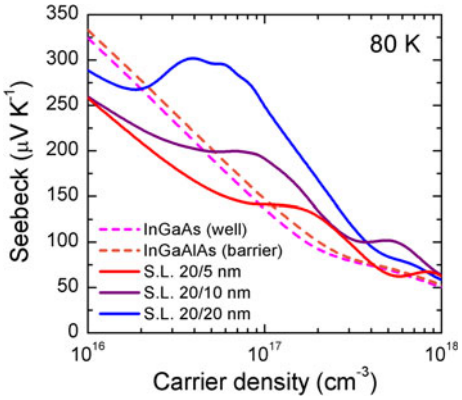

Fig. 5. Seebeck coefficient in the cross-plane direction of InGaAs/InGaAlAs (10% Al) superlattices with three different barrier widths in comparison with that of bulk InGaAs and InGaAlAs (10% Al) as a function of carrier density at 80 K (color figure online).

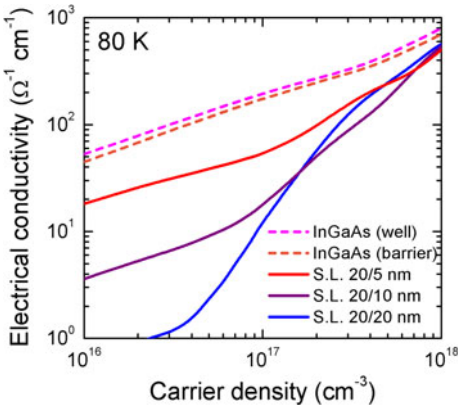

Fig. 6. Electrical conductivity in the cross-plane direction of InGaAs/InGaAlAs (10% Al) superlattices with three different barrier widths in comparison with that of bulk InGaAs and InGaAlAs (10% Al) as a function of carrier density at 80 K (color figure online).

2.4 μW/cm K^2 at the doping level of 7×10^{17} cm^{-3} for the 10-nm-barrier superlattice at 80 K. This represents about a 10% power factor enhancement in comparison with the bulk value at the equivalent doping level. However, the optimal power factor for bulk material is found to be 5.6 μW/cm K^2 at the doping level of 2×10^{16} cm^{-3}, which is much higher than the maximum power factor calculated for the superlattices. Further optimization of the superlattice structures may be possible to further enhance the power factor, but the main limitation on power factor enhancement in miniband transport comes from the group velocity reduction at the low doping levels where the optimal bulk power factor is achieved.

Typically, the optimal Fermi level is about similar for bulk and superlattices within $\sim k_B T$ but the Fermi level of superlattices in reference to the conduction-band minimum of barriers.[9,10] When the superlattice transport is optimized, the Seebeck coefficient can be enhanced at the same time that the group velocity is only slightly reduced from the

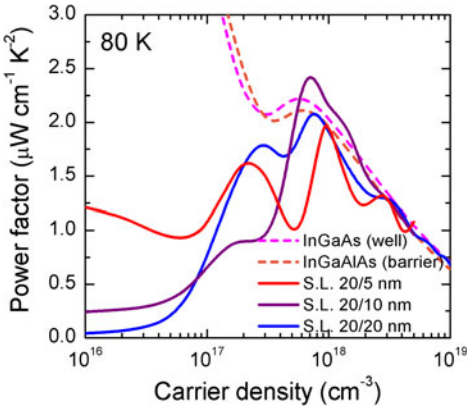

Fig. 7. Power factor in the cross-plane direction of InGaAs/InGaAlAs (10% Al) superlattices with three different barrier widths in comparison with that of bulk InGaAs and InGaAlAs (10% Al) as a function of carrier density at 80 K (color figure online).

bulk value near the edge of the barrier conduction-band minimum. However, the required doping level, higher than in the bulk, makes the impurity scattering stronger and thus the electron mobility smaller. This is particularly true for III–V semiconductor superlattices because impurity scattering is dominant in these materials at low temperatures. This problem may be resolved in two cases: (1) use materials in which the impurity scattering is weak, and (2) the barrier height of the superlattices is small and comparable to $k_B T$ (only $\sim$7 meV at 80 K), making the optimal electron concentration of the superlattices not much higher than that of bulk materials, so that the electron scattering rate is similar. In the latter case, the first miniband still needs to align with the barrier height to achieve the largest Seebeck enhancement.

It is noted that the use of the bulk electron momentum scattering time in calculating the superlattice transport properties can be an error source in this work. Accurate treatment of the scattering mechanisms in superlattices may include separation of momentum into in-plane and cross-plane directions using the modified effective mass and DOS. Surface roughness at layer interfaces and imperfect crystal within layers such as defects and dislocations are the sources of additional scattering of electron momentum. The former can also break the coherence of multiple periods and thus change the miniband formation.

CONCLUSIONS

We studied miniband transport in InGaAs/InGaAlAs III–V semiconductor superlattices in cross-plane direction for efficient thermoelectric energy conversion applications. To estimate the miniband transport accurately, potential bending due to charge transfer between well and barrier layers is included by a self-consistent method to solve the coupled Schrödinger equation and Poisson equation. The cross-plane Seebeck coefficient shows an

oscillating behavior with varying doping density, depending on the Fermi level position relative to the minibands and the forbidden gaps. It is shown that the Seebeck coefficient can be significantly enhanced when the Fermi level is aligned with the edges of the minibands at low temperatures. However, group velocity suppression accompanies the Seebeck enhancement in miniband transport, so that careful design of the superlattice structure is necessary to achieve the largest power factor enhancement.

ACKNOWLEDGEMENT

This work was partially supported by DARPA/ NMP and ARPA-E.

REFERENCES

1. G. Chen and M. Neagu, *Appl. Phys. Lett.* 71, 2761 (1997).
2. T. Koga, S.B. Cronin, M.S. Dresselhaus, J.L. Liu, and K.L. Wang, *Appl. Phys. Lett.* 77, 1490 (2000).
3. B. Poudel, Q. Hao, Y. Ma, Y. Lan, A. Minnich, B. Yu, X. Yan, D. Wang, A. Muto, D. Vashaee, X. Chen, J. Liu, M.S. Dresselhaus, G. Chen, and Z. Ren, *Science* 320, 634 (2008).
4. K.F. Hsu, S. Loo, S.F. Guo, W. Chen, J.S. Dyck, C. Uher, T. Hogan, E.K. Polychroniadis, and M.G. Kanatzidis, *Science* 303, 818 (2004).
5. W. Kim, J. Zide, A. Gossard, D. Klenov, S. Stemmer, A. Shakouri, and A. Majumdar, *Phys. Rev. Lett.* 96, 045901 (2006).
6. L.D. Hicks and M.S. Dresselhaus, *Phys. Rev. B* 47, 12727 (1993).
7. A. Shakouri, C. LaBounty, P. Abraham, J. Piprek, and J. Bowers, *Mater. Res. Soc. Symp. Proc.* 545, 449 (1999).
8. L. Friedman, *J. Phys. C* 17, 3999 (1984).
9. D. Vashaee, Y. Zhang, A. Shakouri, G. Zeng, and Y.J. Chiu, *Phys. Rev. B* 74, 195315 (2006).
10. Z. Bian, M. Zebarjadi, R. Singh, Y. Ezzahri, A. Shakouri, G. Zeng, J.-H. Bahk, J.E. Bowers, J.M.O. Zide, and A.C. Gossard, *Phys. Rev. B* 76, 205311 (2007).
11. W. Kim, S.L. Singer, A. Majumdar, D. Vashaee, Z. Bian, A. Shakouri, G. Zeng, J.E. Bowers, J.M.O. Zide, and A.C. Gossard, *Appl. Phys. Lett.* 88, 242107 (2006).
12. G. Zeng, J.M.O. Zide, W. Kim, J.E. Bowers, A.C. Gossard, Z. Bian, Y. Zhang, A. Shakouri, S.L. Singer, and A. Majumdar, *J. Appl. Phys.* 101, 034502 (2007).
13. K.K. Choi, S.V. Bandara, S.D. Gunapala, W.K. Liu, and J.M. Fastenau, *J. Appl. Phys.* 91, 551 (2002).
14. I. Vurgaftman, J.R. Meyer, and L.R. Ram-Mohan, *J. Appl. Phys.* 89, 5815 (2001).
15. H.T. Grahn, *Semiconductor superlattices: growth and electronic properties* (Singapore: World Scientific, 1995).
16. L.I. Schiff, *Quantum Mechanics* (New York: McGraw-Hill, 1949).
17. J.-H. Bahk, Z. Bian, M. Zebarjadi, J.M.O. Zide, H. Lu, D. Xu, J.P. Feser, G. Zeng, A. Majumdar, A.C. Gossard, A. Shakouri, and J.E. Bowers, *Phys. Rev. B* 81, 235209 (2010).